September 2008
SLAC-PUB-13391

Measurements of Coherent Synchrotron Radiation and its Impact on the LCLS Electron Beam*

K.L.F. Bane, F.-J. Decker, Y. Ding, D. Dowell, P. Emma, J. Frisch, Z. Huang†, R. Iverson, C. Limborg-Deprey, H. Loos, H.-D. Nuhn, D. Ratner, G. Stupakov, J. Turner, J. Welch, J. Wu
Stanford Linear Accelerator Center, Stanford, CA 94309, USA

Abstract

In order to reach the high peak current required for an x-ray FEL, two separate magnetic dipole chicanes are used in the LCLS accelerator to compress the electron bunch length in stages. In these bunch compressors, coherent synchrotron radiation (CSR) can be emitted-induced either by a short electron bunch, or by any longitudinal density modulation that may be on the bunch. We present measurements, simulations, and analysis of 1) the CSR-induced energy loss, 2) the related transverse emittance growth, and 3) the microbunching-induced CSR directly observed at optical wavelengths.

INTRODUCTION

Coherent synchrotron radiation (CSR) is one of the most challenging issues associated with the design of bunch compressor chicanes required for an x-ray free-electron laser (FEL). In recent years, effects of CSR on electron beam qualities have been studied extensively in theory and simulations (see, e.g., Ref. [1] for a recent review). Experimental studies of CSR effects are relatively sparse because adequate beam quality is not commonly available. Examples of previous measurements can be found in Refs. [2, 3]. In this paper, we present detailed measurements of CSR effects at the Linac Coherent Light Source (LCLS) and compare the results with tracking studies. We also present direct observations of CSR at optical wavelengths, evidently due to the modulated beam current (microbunching).

Figure 1 shows a schematic of the LCLS linacs and two bunch compressors (BC1 & BC2). Both compressors are four-dipole chicanes and are motorized so that the center two dipoles can be translated on a stage to match the bend fields and electron energy. The injector through BC1 was successfully commissioned in 2007 [4], and some preliminary results of BC1 compression and emittance growth were reported in Ref. [6]. The entire accelerator including BC2 has just concluded commissioning in 2008 [5]. A relatively low charge of 250 pC is used to tune up the machine and to perform these CSR measurements. The nominal linac and bunch compressor parameters at this charge are listed in Tables 1 and 2. The rms bunch length is compressed from 750 μm to about 100 μm after BC1, and then to about 8 μm after BC2 to reach about 2.5 kA final current under the normal operating condition.

* Work supported by the U.S. DOE contract DE-AC02-76SF00515.
† zrh@slac.stanford.edu

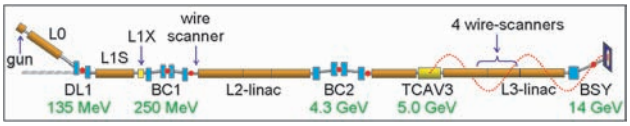

Figure 1: LCLS accelerator layout showing BC1, BC2, transverse RF cavity (TCAV3), and screen at end of linac.

Table 1: Nominal beam and linac parameters for 250-pC bunch charge operation.

Parameter	Symbol	Value	Unit
Injector bunch length (rms)	σ_{z0}	~750	μm
Injector norm. emit. (x/y)	$\gamma\epsilon_0$	~0.7	μm
L1S RF phase (2856 MHz)	ψ_1	-22	deg-S
L1X RF phase (11.4 GHz)	ψ_X	-160	deg-X
L1X RF voltage	V_X	20	MV
L2 RF phase	ψ_2	-37	deg-S
L3 RF phase	ψ_3	0	deg-S
Final electron energy	E_f	13.64	GeV
Final bunch length (rms)	σ_{zf}	~10	μm
Final norm. emit. (x/y)	$\gamma\epsilon_f$	~1.3/0.7	μm

Table 2: BC1 and BC2 chicane parameters at 250 pC.

Parameter	Symbol	BC1	BC2	Unit
Electron energy	E_0	0.25	4.3	GeV
Energy spread (rms)	σ_E/E_0	1.4	0.38	%
Momentum compaction	R_{56}	-45.5	-24.7	mm
Chicane total length	L_T	6.5	23	m
Bend angle per dipole	$\|\theta\|$	5.4	2.0	deg
Eff. length per dipole	L_B	0.20	0.54	m
Dipole bending radius	ρ	2.1	15.5	m
B1 to B2 (=B3 to B4)	ΔL	2.43	9.87	m
Dispersion at center	$\|\eta\|$	247	363	mm
Translation range	Δx	0-30	0-52	cm

BC1 RESULTS

Measurements

As shown in Table 1, the typical rms bunch length at 135 MeV is measured at 750 μm using a transverse deflecting cavity located in the injector area, and the normalized emittances in x and y planes are about 0.7 μm routinely measured with an optical transition radiation (OTR) screen and a wire scanner before a 35° Dog-Leg (DL1). In order to study the CSR effects on BC1 compression, the incoming energy chirp of the electron bunch is varied by adjusting the L1S phase from -20 to -30 degrees while holding the energy and BC1 R_{56} constant at -45.5 mm. The short x-band section (L1X) used to linearize the longitudinal phase

Presented at the 30th International Free Electron Laser Conference FEL, 8/24/2008 to 8/29/2008, Gyeongju, Republic of Korea

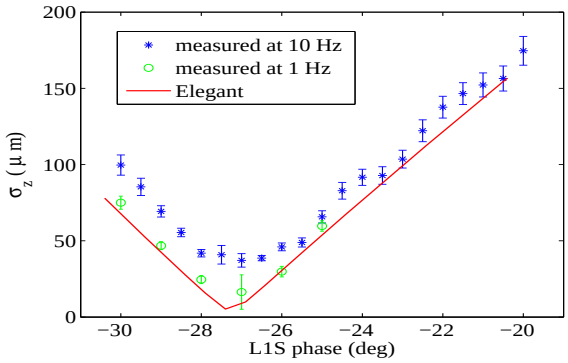

(a) Compressed bunch length with BC2 OFF.

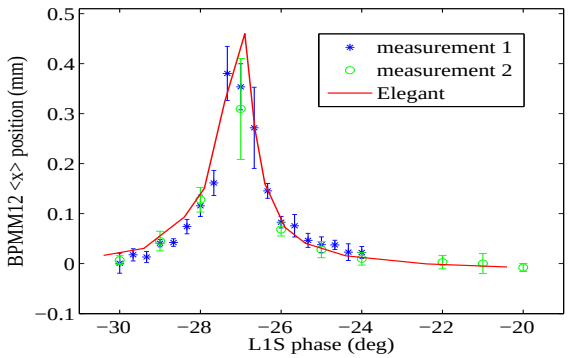

(b) BPMM12 X-position readout after BC1

Figure 2: BC1 compression measurements and simulations (solid curves) vs. L1S phase (zero phase means on crest).

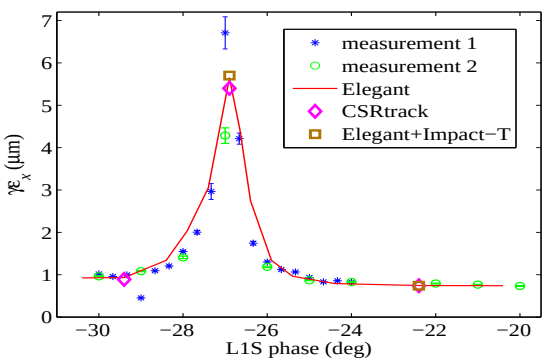

(a) Horizontal emittance after BC1.

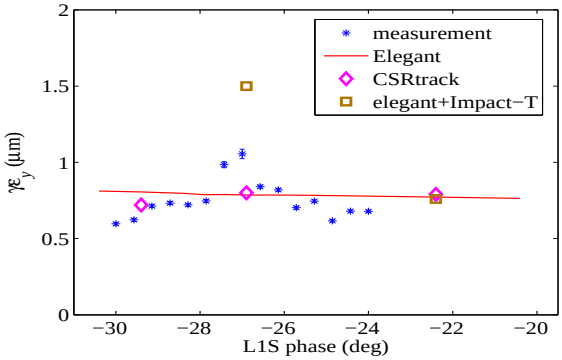

(b) Vertical emittance after BC1.

Figure 3: Measured and simulated transverse emittances after BC1 vs. L1S phase.

space is also held constant in phase and amplitude. To measure the absolute bunch length after BC1, we switch off BC2 magnetic fields and chirp the bunch vertically using a transverse deflecting cavity located at 5 GeV (TCAV3 in Fig. 1). The phosphor screen located at the beam switch yard (BSY) after the L3 linac records the vertical beam size, which is then converted to the rms bunch length due to the imposed $y - z$ correlation by TCAV3. The phosphor screen exhibits some persistence of beam images at higher bunch repetition rates. Thus, the measured bunch lengths shown in Fig. 2(a) are usually longer at 10-Hz than at 1 Hz. Figure 2(a) also shows that the bunch is under-compressed above -27 degree and over-compressed below -27 degree, with the minimum measured rms bunch length of about 10 μm at the full compression.

In a dipole magnet, a short Gaussian bunch radiates coherently with the average energy loss per electron per unit length given by $dE/ds \approx 1.8N(e)^2/(\rho^{2/3}\sigma_z^{4/3})$ [7], where $N = 1.56 \times 10^9$ is total number of electrons (at 250 pC), and $\rho = 2.1$ m is the BC1 dipole bending radius (see Table 2). A compressed bunch with the rms bunch length σ_z traversing the last dipole of BC1 (about 0.2 m in length) can induce a significant energy loss due to CSR (about 2 MeV for $\sigma_z = 10$ μm at 250 pC). Since the energy loss occurs primarily in the last dipole, the bunch will be kicked horizontally and will execute a betatron oscillation after compression. A BPM after BC1 (BPMM12) shows the expected horizontal steering effect due to CSR (see Fig. 2(b)), which can be utilized in a quick scan to identify the full compression phase without bunch length measurements.

Associated with the CSR energy loss, the bunch energy spread can increase in the chicane, giving rise to the horizontal emittance growth after the chicane. A quadrupole right after BC1 and a wire scanner $\sim$ 3 m downstream (shown in Fig. 1) are used to measure the projected emittances in both x and y directions with the quad-scan technique. Two separate measurement results for horizontal emittances and another measurements for vertical emittances are shown in Figs. 3(a) and 3(b). In addition to the very pronounced peak in horizontal emittance at the full compression, a small vertical emittance increase (about 50%) is also visible from Fig. 3(b). Note that BC1 normally operates at -22 degree with a compression factor of about 6. The transverse emittances are unaffected by CSR at this operating point. Note also that the transverse emittances almost fully return to the uncompressed level below -29 degree, i.e., when the bunch is over-compressed. Figure 4 shows the measured and simulated horizontal profiles of the compressed beam from the wire scanner for the operating phase and the full compression phase, respectively. The horizontal profile at full compression is much larger and very distorted with amplified shot-to-shot position jitter.

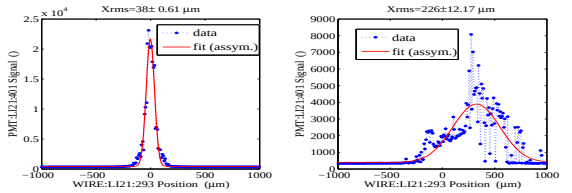

(a) $\psi_1 = -22°$ (measurement) (b) $\psi_1 = -27°$ (measurement)

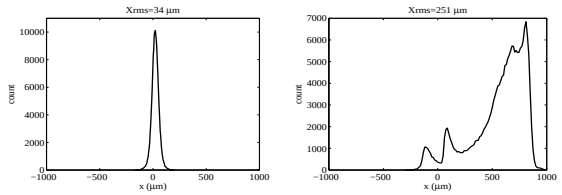

(c) $\psi_1 = -22°$ (simulation) (d) $\psi_1 = -27°$ (simulation)

Figure 4: Measured and simulated horizontal beam profiles at the post-BC1 wire scanner for two L1S phases.

Simulations

Multi-particle simulations are used to compare with these measurements. First the injector (up to DL1 in Fig. 1) is modeled using the *IMPACT-T* [8] space charge code with one million macroparticles. The simulated normalized emittances at the injector end yield the measured level of 0.7 μm, while the simulated bunch length is chosen to match the measured rms value of 750 μm. These macroparticles are input into *Elegant* [9] and tracked through BC1 with a 1-D CSR model for different L1S phases. As shown in Fig. 2(a), a phase shift of -0.4 degree is added in the simulation curve to fit with measurements of the compressed bunch length. This phase shift may come from rf drift during the measurements or the small uncertainly in the initial phase. The CSR steering effect agrees well with the BPMM12 readout (see Fig. 2(b)). In addition, *Elegant* simulated horizontal and vertical emittances (red curves) are shown in Figs. 3(a) along with the experimental data. To check the 1-D CSR model of *Elegant*, *CSRTrack* [10] with a 2-D (x-z) CSR algorithm ("g_to_m" method) is also used to track BC1 region for three L1S phases (when the beam is under compressed, fully compressed, and over compressed). Good agreement is found between measured horizontal emittances and simulation results from both *Elegant* and *CSRTrack*. The simulated rms bunch length from *CSRTrack* also agrees with *Elegant* very well. Figure 4 shows the measured and simulated wire scanner profiles from *Elegant* are quite comparable. Since no vertical self-force is present in these two codes, *Elegant* and *CSRTrack* simulations do not show any vertical emittance growth. However, *Elegant* simulations indicate a peak current of $\sim$ 20 kA at full compression. Transverse space charge force from this high-current spike may increase the vertical emittance in the 3-m drift section after BC1 before the beam reaches the wire scanner. Using *Impact-T* at the exit of BC1 to simulate space charge effects in this 3-m drift section, we observe an increase of the vertical emittance at full compression that is similar to the measurements (see Fig. 3(b)).

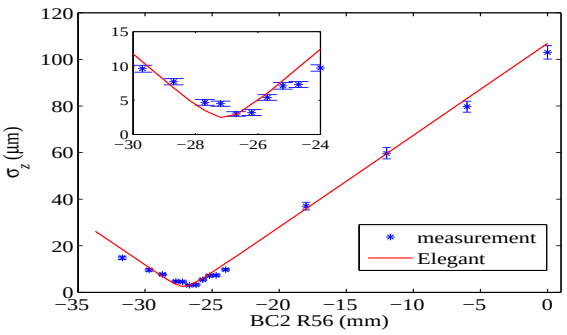

(a) Compressed bunch length after BC2.

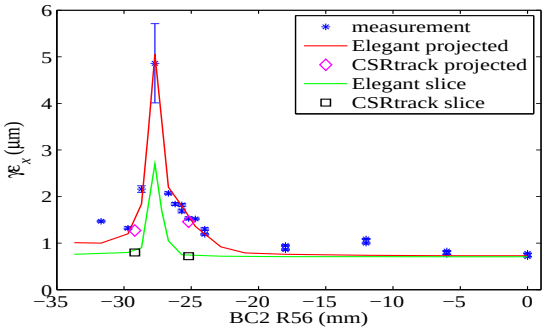

(b) Horizontal emittance after BC2.

Figure 5: BC2 bunch length compression and emittance growth measurements and simulations.

BC2 RESULTS

Bunch length and emittance measurements

When BC2 is switched on, we can vary the L2-linac phase to measure the BC2 bunch compression and its effect on the beam. The results are less reliable compared to the previous BC1 studies because the klystrons used for BC2 energy feedback may steer the beam transversely when L2 phase is adjusted. Instead, we vary the strength of the BC2 chicane while holding the L2 linac phase at -37 degree. The compressed bunch length is measured with the TCAV3 transverse RF deflector at a 1-Hz beam rate. The projected transverse emittances are measured with 4 wire scanners near the end of the linac at about 10 GeV (see Fig. 1). Figures 5(a) and 5(b) show the measured bunch length and horizontal emittance as a function of BC2 chicane strength. The rms bunch length measurements extend down to 2 μm near full compression. When BC2 is switched off, the horizontal emittance returns to the same level as the vertical emittance (not shown), both at 0.7 μm level under nominal BC1 compression. This confirms the emittance preservation through the linac when BC2 compression is absent. However, when BC2 operates at the nominal strength with $R_{56} = -24.7$ mm at 250 pC, the horizontal projected emittance is almost doubled due to CSR. *Elegant* tracking of the entire accelerator including wakefields, longitudinal space charge in the linac, and CSR in BC1 and BC2 confirms the CSR emittance growth in BC2 as shown in Fig. 5(b) (red curve). The initial beam configurations are similar to the

previous BC1 simulations, and -1 degree is added to the L2 phase in these simulations in order to match the bunch length measurements as shown in Fig. 5(a). Simulations suggest that most of the emittance increase comes from the high-current leading and trailing spikes formed near the end of BC2, while the slice emittance in the core part of bunch is unaffected at the nominal BC2 compression as shown by the green curve in Fig. 5(b). These *Elegant* results are confirmed with *CSRtrack* simulations of BC2.

Direct observations of CSR on an OTR screen

As discussed above, wire scanners instead of OTR screens are used to measure the compressed beam profiles and transverse emittances. All OTR screens after DL1 are compromised by a strong coherent OTR (COTR) signal due to possible high-frequency longitudinal structure on the electron beam and hence cannot be used for accurate beam profile measurements [4, 11]. Nevertheless, CSR signals generated inside a dipole, horizontally separated from COTR signals, are observed on an OTR screen (OTR21, shown in Fig. 1 as a red dot in the middle of BC2) by adjusting the strength of a horizontal-focusing quadrupole right in front of BC2 (QM21). The energy-chirped electron beam entering BC2 is dispersed horizontally in the middle of BC2. Thus, the COTR signal on OTR21 emitted by such a beam has a large aspect ratio of the transverse spot size as shown in Fig. 6(a) when QM21=34 kG (nominal value). As we decrease QM21 strength to 27 kG, a CSR signal with a more round transverse spot size appears in Fig. 6(b). It becomes further horizontally separated from COTR at even lower QM21 values as shown in Figs. 6(c) and 6(d). In fact, a part of CSR signal is clipped off by the OTR screen holder in Fig. 6(d).

Since the OTR camera is sensitive to optical radiation ranging from 350 nm to about 1 μm in wavelength, the observed CSR signal most likely comes from the beam longitudinal density modulation (microbunching) instead of the overall bunch shape with an rms bunch length of about 50 μm (rms) in the middle of BC2 at the nominal compression. The evolution of a microbunched beam in a chicane under the influence of CSR can be described by an integral equation [12, 13]. Neglecting a small level of CSR amplification of microbunching, the amplitude of density modulation in a chicane is determined by x-z (R_{51}) and x'-z (R_{52}) transport coefficients as in Eqs. (26) and (41) of Ref. [13]. Thus, varying the horizontal beam divergence through QM21 changes the microbunching amplitude through these coefficients inside the chicane. If the maximum of the density modulation amplitude is reached inside the second dipole, strong CSR signal emitted from that location will reach OTR21, shifted to the $+x$ direction from the screen center where the COTR signal is generated by the passing electron beam. This hypothesis is tested with numerical calculations based on the BC2 lattice functions. The calculated shifts of CSR center to COTR center are 0, 5, and 7 mm for QM21=27, 23, and 21 kG, respectively. These numbers agree with estimations from Figs. 6(b), 6(c) and 6(d). At QM21=34 kG, microbunching is strongly suppressed in the second dipole, and no CSR signal is observed in this case. Finally, the CSR spot size is also consistent with the estimation based on the radiation opening angle at the optical wavelength.

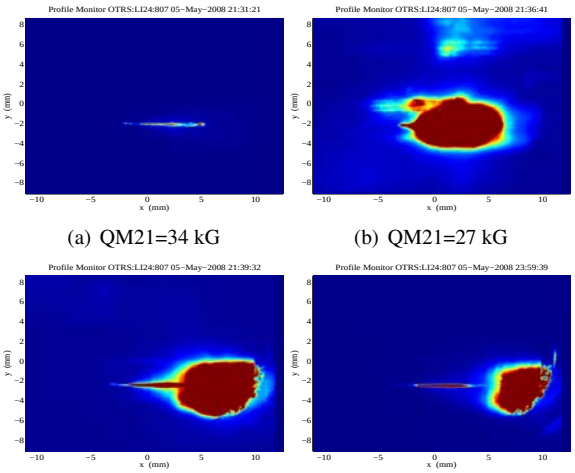

(a) QM21=34 kG (b) QM21=27 kG

(c) QM21=23 kG (d) QM21=21 kG

Figure 6: Optical radiation pattern observed on OTR21 near the beginning of the third dipole in BC2 vs. pre-BC2 quadrupole strength (QM21).

SUMMARY

We have presented measurements of CSR-induced energy loss and related transverse emittance growth in both LCLS bunch compressors, and observed CSR emission induced by the microbunched beam. These measurements are consistent with simulations and analysis. The addition of a Landau-damping laser heater [14] in late 2008 should suppress these high-frequency beam structures and may also reduce the emittance growth in BC2.

REFERENCES

[1] G. Bassi *et. al.*, Nucl. Instrum. Methods A **557**, 189 (2006).

[2] H.H. Braun *et. al.*, Phys. Rev. ST-AB **3**, 124402 (2000).

[3] M. Borland, J. Lewellen, PAC2001, 2823 (2001).

[4] R. Akre *et. al.*, Phys. Rev. ST-AB **11**, 030703 (2008).

[5] R. Akre *et. al.*, these FEL2008 Proceedings.

[6] K. Bane *et. al.*, PAC2007, 807 (2007).

[7] J.S. Nodvick and D.S. Saxon, Phys. Rev. **96**, 180 (1954).

[8] J. Qiang *et. al.*, Phys. Rev. ST-AB **9**, 044204 (2006).

[9] M. Borland, ANL/APS LS-287 (2000).

[10] M. Dohlus, T. Limberg, FEL2004, 18 (2004).

[11] J. Frisch *et. al.*, 13^{th} Beam Instrum. Workhshop, Lake Tahoe, CA (May, 2008).

[12] S. Heifets, G. Stupakov, S. Krinsky, Phys. Rev. ST-AB **5**, 064401 (2002).

[13] Z. Huang, K.-J. Kim, Phys. Rev. ST-AB **5**, 074401 (2002).

[14] Z. Huang *et. al.*, Phys. Rev. ST-AB **7**, 074401 (2004).